Carbon-mediated visible-light clay-Fe 2 O 3 -graphene oxide catalytic nanocomposite for the removal of steroid estrogens from water

Article *in* Journal of Water Process Engineering · December 2020

DOI: 10.1016/j.jwpe.2020.101865

CITATION
1

READS
154

12 authors, including:

Ajibola Bayode
Redeemer's University
6 PUBLICATIONS **36** CITATIONS
SEE PROFILE

Dayana Moscardi Santos
University of São Paulo
28 PUBLICATIONS **406** CITATIONS
SEE PROFILE

Dr Martins O. Omorogie
Redeemer's University
56 PUBLICATIONS **540** CITATIONS
SEE PROFILE

Olumide Olukanni
Redeemer's University
43 PUBLICATIONS **541** CITATIONS
SEE PROFILE

Contents lists available at ScienceDirect

Journal of Water Process Engineering

journal homepage: http://ees.elsevier.com

Carbon-mediated visible-light clay-Fe_2O_3–graphene oxide catalytic nanocomposite for the removal of steroid estrogens from water

Ajibola A. Bayode [a,b,c], Dayana M. dos Santos [c], Martins O. Omorogie [a,b], Olumide D. Olukanni [b,d], Roshila Moodley [e], Olusola Bodede [e], Foluso O. Agunbiade [f], Andreas Taubert [g], Andrea S.S. de Camargo [h], Hellmut Eckert [h], Eny Maria Vieira [c], Emmanuel I. Unuabonah [a,b,*]

[a] Department of Chemical Sciences, Faculty of Natural Sciences, Redeemer's University, PMB 230, Ede, Osun State, Nigeria
[b] African Centre of Excellence for Water and Environmental Research (ACEWATER), Redeemer's University, PMB 230, Ede, 232101, Osun State, Nigeria
[c] Laboratório de Química Analítica Ambiental e Ecotoxicologia (LaQuAAE), Departamento de Química e Física Molecular, Instituto de Química de Sao Carlos, Universidade de Sao Paulo, Sao Carlos, Brazil
[d] Department of Biochemistry, Faculty of Basic Medical Sciences, Redeemer's University, PMB 230, Ede, Osun State, Nigeria
[e] School of Chemistry and Physics, University of KwaZulu-Natal, Westville Campus, Durban, 4000, South Africa
[f] Department of Chemistry, University of Lagos, Lagos, Nigeria
[g] Institute of Chemistry, University of Potsdam, D-14476, Potsdam, Germany
[h] Sao Carlos Institute of Physics, University of São Paulo, Avenida Trabalhador Sãocarlense 400, São Carlos, SP, 13566-590, Brazil

ARTICLE INFO

Keywords
Visible-light
Photocatalyst
Steroid estrogens
Wastewater treatment
Carbon
Graphene oxide
Hematite

ABSTRACT

This study reports the development of an efficient photosensitive nanocomposites made from Clay, Fe_2O_3, and Graphene oxide (GO). These nanocomposites were used for the removal of steroid estrogens (E1, E2, E3 and EE2) from water under visible-light. The use of these photocatalytic nanocomposites lead to complete oxidation of the steroid estrogens at >80 % even under simultaneous presence of all estrogens in water. Complete mineralization was obtained for these estrogens with the range of 58–73 %. The presence of Fe-oxide in the nanocomposites increased the photocatalytic efficiency but addition of GO further improved the photocatalytic efficiency. This improved efficiency was further doubled when the nanocomposites were prepared with a carbon source (*carica papaya* seeds). The presence of carbon in the nanocomposite matrix was confirmed using X-ray Photoelectron Spectroscopy and Elemental Analysis. The main contributors to photocatalytic efficiency of the nanocomposites are superoxide radicals ($\cdot O_2^-$) and holes (h^+). Under competitive conditions, the catalysts are still active although the extent of estrogen oxidation is somewhat lower. Changes in the ionic strength did not significantly influence the efficiency of the photocatalyst. This signifies that adsorption only plays a minor role in estrogen removal from water. Toxicity tests show that the treated water is safe for human consumption and the most efficient nanocomposite can be recycled three times without any significant loss of performance. Overall, the nanocomposite shows high potential for the effective removal of a cocktail of estrogens in raw wastewater, tap and rain water, attaining contamination levels that are within WHO safe limits.

1. Introduction

Over the past decades, industrialization and urbanization have led to an increased amount of endocrine-disrupting chemicals (EDCs) released into water bodies and the environment. This poses serious environmental and health challenges due to high toxicity, persistence, and estrogenicity of EDCs [1,2].

The most important groups of EDCs are the natural and synthetic hormones, pesticides, pharmaceuticals, personal care products, and some heavy metals [3,4]. Estrogens are primary female sex hormones that are responsible for the development and regulation of the female reproductive system and secondary sex character [3,5]. Of these estrogens, estrone (E1), 17β-estradiol (E2), estriol (E3), and 17-α ethynyl estradiol (EE2) (Fig. 1) are major contributors to estrogenicity and ecological risk [6,7] and are therefore the major focus of this study.

E1, E2, and E3 are endogenous (naturally occurring) estrogens present in women while EE2 is the synthetic derivative of estradiol (E2). It is used as an active ingredient in post-menopausal hormonal appurtenances and oral contraceptive pills [6].

* Corresponding author at: Department of Chemical Sciences, Faculty of Natural Sciences, Redeemer's University, PMB 230, Ede, Osun State, Nigeria.
E-mail address: unuabonahe@run.edu.ng (E.I. Unuabonah)

https://doi.org/10.1016/j.jwpe.2020.101865
Received 29 September 2020; Received in revised form 10 November 2020; Accepted 3 December 2020
Available online xxx
2214-7144/

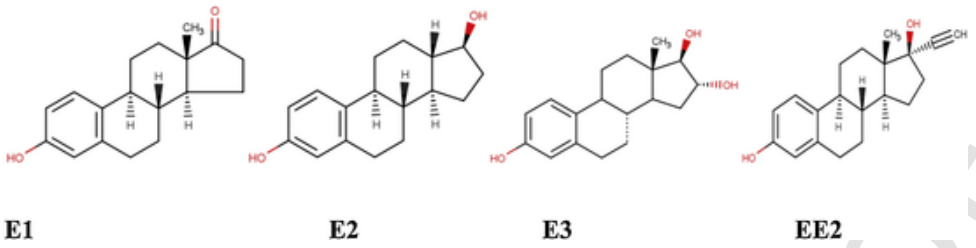

Fig. 1. Chemical Structures of the Steroid Hormones E1, E2, E3 and EE2.

These estrogens occur in the natural environment, such as seawater [8], surface water [9], or soil, [10] and reports have linked them to breast cancer, ovarian cancer, feminization in fishes, low sperm count in adult males, endometriosis, obesity, cardiovascular endocrinology, and fibroid even at trace concentrations [11–13].

Approximately 30,000 kg of natural steroidal estrogens (E1, E2, and E3) and an additional 700 kg of synthetic estrogens (EE2) solely from birth control pills are discharged into water bodies yearly [11]. Humans and animals largely excrete these estrogens *via* urine and faeces as active free forms or inactive glucuronide and sulfate conjugates with animals excreting more than humans [11]. Other sources of these estrogens in the environment include effluents from the wastewater treatment plant and animal waste [14,15].

In the developing world, especially in most countries in Africa, municipal water treatment is non-existent. The population depends generally on streams (surface water), groundwater, point-of-use water treatment systems, and packaged water as sources of drinking water. Most of these sources still provide drinking water with some levels of estrogens either because the water is polluted *via* transport to the underground drinking water sources or because they are not adequately treated before they are sold to consumers. Both situations are primarily caused by the high-cost of purchase and maintenance of state-of-the-art water treatment technology such as membrane filtration, ultrafiltration, nanofiltration and reverse osmosis [16–18] which are best suited for the removal of these estrogens from water.

Elimination of these highly toxic molecules, even at low concentration, from wastewater is challenging, especially because of their low bioavailability, persistence, and complicated structures [19]. Traditional water treatment plants are not designed to remove or reduce these hormones in drinking water effectively [20]. This prompted the development of additional, more specific and more efficient techniques for their removal from water. Some of these techniques include ozonation [21], the use of activated carbon for adsorption [5], biological degradation [14], advanced oxidation processes (AOPs) including free radical oxidation [22], electrochemical oxidation [23], sonolysis [24], and membrane technology [25]. Of these techniques, electrochemical oxidation is effective but slow and requires frequent replacement of electrodes. The membrane approach is the most efficient as well as the most expensive one. Moreover, it also requires frequent membrane replacements due to fouling. The adsorption technique is useful but limited by the molecular size of the estrogens and their very low concentration in environmental samples. The AOPs including photocatalysis technique, can generate reactive oxygen species that mineralize organic contaminants and their intermediates to CO_2 and H_2O, have been used mostly for removal of estrogen from water under ultraviolet radiation [22,26,27].

The present study describes new visible-light active photocatalytic nanocomposites generated from Kaolinite, crushed *Carica papaya* seeds, 3-aminopropyltriethoxysilane (APTES), hematite (Fe_2O_3) and graphene oxide (GO), for the effective oxidation and subsequent mineralization of the steroid hormones, estrone, 17β-estradiol, estriol, and ethinyl estradiol. The use of Kaolinite and crushed *Carica papaya* seeds is motivated by the demand for low-cost, efficient, visible-light-driven, and sustainable photocatalysts, which function without the additional expenses for supplemental UV lamps and power supplies.

The photocatalytic system designed in the present study contains the following components; (1) kaolinite serving as a low-cost matrix support, (2) graphene oxide known to be very effective as a photocatalyst in visible light [28], (3) Fe_2O_3, with its ability to absorb a large portion of visible solar spectrum, good chemical stability in aqueous medium, low cost, abundance and non-toxic nature, (4) *carica papaya* seeds, which serve as a carbon source that assists in the creation of mesoporosity in the composite and reduce the rate of recombination of photogenerated e-/h + pair generated by Fe_2O_3-Graphene oxide composite under visible light [29], and (5) APTES which serves as a source of nitrogen atoms, which broaden the composites' absorption spectrum in the visible region considering that the present study is to be conducted under laboratory fluorescent lamps as the excitation source in the photocatalytic process. It is the aim of this study to show the synergy between these components of prepared photocatalytic nanocomposite material and to what extent they enhance photoactivity.

The prepared photocatalyst has advantages such as the use of environmentally friendly chemical for synthesis and synthesis ease, thus making it cost effective and easily scalable. To the authors best knowledge this is one of the first reports on the use of carbon-mediated clay- Fe_2O_3-GO visible-light catalysts for the mineralization of estrogens in water. The photocatalytic materials developed in this study hold promise for small scale treatment of drinking water treatment, mostly needed in developing countries.

2. Materials and methods

2.1. Materials and precursors

Materials and precursors used for the preparation of composite materials in this study are shown in section S.1 (SI document).

2.2. Material synthesis

Kaolinite clay and the biomass (crushed *Carica papaya* seeds) were pretreated and purified as previously reported [30]. The nomenclature, composition and ratio of components for the various materials prepared in this study are shown in Table 1.

However, the details of preparation for the various composites are presented in the supporting information **(S 2.1–2.5).** The graphene oxide was synthesized in the laboratory from graphite using Hummer's method [31]. These materials were used for preliminary study to ascertain the influence of each of the components and their various combinations on the removal efficiency of the nanocomposites for steroid estrogens in water. Similar method described in section 2.5 was used but samples were only withdrawn and analyzed for the presence of steroid estrogen after 720 min.

2.3. Characterization of the nanocomposite photocatalysts

Electron microscopy was done on a Zeiss FEG-SEM Ultra plus field emission gun scanning electron microscope (SEM) operated at 5 kV and

Table 1
Information on the Nomenclature, composition and ratio of components of various materials prepared in the study.

Nanocomposite nomenclature	Composition	[a]Ratio of components
PSK	Crushed *carica papaya* seeds, kaolinite, $ZnCl_2.6H_2O$, 20 mL 0.1 M NaOH	1:1:2
KGO	Kaolinite, Graphene oxide	2:1 respectively +50 mL methanol
N-K	Kaolinite in 2:1 of Toluene: Water	2 g +3 mL APTES
N-KGO	kaolinite, Graphene oxide	2:1 respectively +3 mL APTES
Fe@KGO	$FeCl_2.4H_2O$, $FeCl_3.6H_2O$, kaolinite, Graphene oxide	1.6:4.4:2:1 respectively
Fe@K	$FeCl_2.4H_2O$, $FeCl_3.6H_2O$, kaolinite	1.6:4.4:2 respectively
N-Fe@K	$FeCl_2.4H_2O$, $FeCl_3.6H_2O$, kaolinite	1.6:4.4:2 respectively +3 mL APTES
N-Fe@KGO	$FeCl_2.4H_2O$, $FeCl_3.6H_2O$, kaolinite, Graphene oxide	1.6:4.4:2:1 respectively +3 mL APTES
Fe@PSK	$FeCl_2.4H_2O$, $FeCl_3.6H_2O$, PSK	1.6:4.4:2 respectively
Fe@PSK@GO	$FeCl_2.4H_2O$, $FeCl_3.6H_2O$, PSK, Graphene oxide	1.6:4.4:2:1 respectively
N-Fe@PSK	$FeCl_2.4H_2O$, $FeCl_3.6H_2O$, PSK	1.6:4.4:2 respectively +3 mL APTES
N-Fe@PSK@GO	$FeCl_2.4H_2O$, $FeCl_3.6H_2O$, PSK, Graphene oxide	1.6:4.4:2:1 respectively +3 mL APTES

[a] Details of how each of these materials were prepared are shown in **section S.2** in the supporting information document.

equipped with an energy-dispersive X-ray (EDX) spectrometer (Aztec Analysis Software, England) as well as on a HR-TEM, JEOL 2100 transmission electron microscope (TEM, field emission gun, 200 kV) equipped with diffraction apertures for selected area electron diffraction (SAED). Infrared spectra were collected on a Perkin Elmer (USA) Spectrum 100 Fourier transform infrared (FTIR) spectrometer with universal attenuated total reflectance (ATR) sampling accessory. Raman spectra were measured on a WITec Alpha 300 RAS Microscope with a 785 nm laser (WITec, Ulm, Germany). Thermogravimetric analysis (TGA) and differential thermal analysis (DTG) was done on a Netzsch TG 209F1 220–10-055-K from 30 to 1000 °C with a heating rate of 10 °C/ min in air. Raman spectroscopy was performed on a WITec Alpha 300 RAS Microscope (WITec, Ulm, Germany). Nitrogen sorption was done on a Quantachrome NOVA1000e BET system. Electron paramagnetic resonance (EPR) spectroscopy was performed at 77 and 298 K using a TE102 rectangular cavity with a microwave power of 2 mW and modulation amplitude of 1 G (EMX plus, Bruker BioSpin, Rheinstetten, Germany). X-ray photoelectron spectroscopy (XPS) was done on a Thermo Scientific K-Alpha spectrometer with a monochromatic Al Kα (1486.6 eV) radiation source.

2.4. Optical properties

The optical properties of the prepared nanocomposites were determined using a Shimadzu UV/Vis spectrophotometer equipped with a solid sample reflectance kit, using $BaSO_4$ as the reference standard and the apparent band gap of the nanocomposites were estimated using the Tauc equation [32].

$$\alpha h\nu = A(h\nu - E_g)^{\frac{1}{2}} \quad (1)$$

where α is the absorption coefficient, h is the Planck's constant, ν is the, light frequency, Eg is the apparent band gap energy, and A is a constant [33].

2.5. Photo-oxidation of steroid estrogens

A kinetic study was performed to determine the efficiencies of the nanocomposites using 90 mL of a solution containing the steroid estrogens (concentration 5 mg/L) with 0.03 g/L of the photocatalytic nanocomposite. The pH of the mixture was adjusted to pH 7.0 using 0.01 M HCl and NaOH respectively. The mixture, in a transparent glass beaker, was agitated for 720 min with 35 W white fluorescent lamps as light source. Previous study of the fluorescent lamp source indicate its absorption in the visible region at wavelengths of 400, 450, 550 and 580 nm [34]. Solution aliquots of 1 mL were withdrawn at specific time intervals. The composites were separated by filtration through 0.45 μm PTFE syringe filters. To ascertain that the filter does not adsorb the estrogens, untreated samples of the steroid estrogens were filtered through the PTFE filter as well. The concentration of the remnant steroid estrogens was determined using high-performance liquid chromatography (HPLC, Agilent 1200 series HPLC-DAD detector at wavelength of 285 nm). Gradient elution was conducted with a mixture of acetonitrile and water spiked with 0.1 % formic acid, (3 m in. 30/70 %; 4 m in. 40/60 %; 10 m in. 45/65 %; 13 m in. 30/70 %) with a flow rate of 1 mL/min, and an injection volume of 20 μL for 12 min. A Zorbax SB-CN (5 μm) reverse phase (4.6 × 250 mm) column was used for separation. The degree of steroid estrogen oxidation was calculated *via*:

$$R(\%) = \frac{C_o - C_e}{C_o} \times 100 \quad (2)$$

where C_o and C_e are the initial and final concentrations of the steroid estrogen (mg/L).

The contribution of adsorption to the estrogen removal process was determined using a similar setup but in the absence of light. Finally, to evaluate the direct influence of laboratory lighting on the removal of these estrogens from water, the same experiment was carried out in the absence of composite material present in the solution. All samples were withdrawn and analyzed after 720 min.

The effect of some variables (composite dose, pH, and initial concentration of steroid hormones, ionic strength and anions) with respect to the photocatalytic process and toxicity test using treated and untreated water effluents were also studied using the nanocomposite with the best efficiency: Fe@PSK@GO. The details of these studies are described in the supporting information document **(S 2.0)** and all analysis of samples were carried out in triplicate.

2.6. Degree of oxidation

The degree of complete oxidation of estrogens after photocatalysis was determined by chemical oxygen demand, COD (determination of the oxygen equivalent of the organic matter of the degraded steroid estrogen effluent) using a Nanocolor® Vario 4 spectrophotometer. The reagents for COD analysis (Solution A $K_2Cr_2O_7$ + H_2SO_4 and Solution B concentrated H_2SO_4 and Ag_2SO_4) and a 2.5 mL treated water sample were mixed in a glass cell and digested in a Nanocolor® Vario 4 digestion reactor for 2 h at 150 °C. After digestion, the mixture was cooled to room temperature, and the COD was measured using the Nanocolor® spectrophotometer. The COD was measured for blank (milli-Q water) used in the preparation of the steroid estrogen solution and for centrifuged treated water samples. The fraction of estrogen completely oxidized was calculated *via*

$$\%\ complete\ Oxidation = \frac{COD_o - COD_e}{COD_o} \times 100 \quad (3)$$

Where, COD_o is the initial COD before degradation and COD_e is the fi-

nal COD after degradation. Results of *% complete oxidation* were subtracted from results obtained from kinetic studies after 720 min. This provided the amount of estrogen actually mineralized to CO_2 and H_2O. All analysis of samples were carried out in triplicate.

2.7. Toxicity test

To test the estrogenicity and toxicity of the treated water, *Ceriodaphnia silvestrii*, a freshwater cladoceran species was used. Further details of the toxicity test are shown in **section S 3.0** in the supporting information document.

2.8. Detection of active species

To identify reactive species generated by the Fe@PSK@GO nanocomposite (the nanocomposite with the best efficiency), a radical trapping study was performed. Reactive species of focus were hydroxyl radical (·OH), superoxide radical ($\cdot O_2^-$), and holes (h^+). To solutions with 5 mg/L of steroid estrogen, 10 mL of an aqueous 0.05 mM isopropanol (IPA) solution, 10 mL of an aqueous 0.05 mM benzoquinone (BQ) and 10 mL of an aqueous 0.05 mM ammonium oxalate (AO) was added and mixed with 0.1 g/L of the nanocomposite. IPA, BQ and AO are used to detect the presence of ·OH, $\cdot O_2^-$ and h^+, respectively, in aqueous systems [32]. All analysis of samples were carried out in triplicate.

2.9. Treatment of natural, treated and environmental waste water

The performance of the most efficient photocatalytic nanocomposite, Fe@PSK@GO, for the photo-oxidation of steroid estrogens (E1, E2, E3 and EE2) in tap water collected from a point-of-use water system in the laboratory, rainwater, and wastewater collected from around the wastewater sewer in the University of São Paulo, São Carlos, Brazil (22.0027 °S, 47.8986 °W), was studied. All samples were collected in amber bottles with Teflon-liner caps. Physicochemical properties (conductivity, temperature, pH and total dissolved solids) were measured initially in the collected samples. Thereafter, the samples were fixed with sulfuric acid (1%, V/V) to prevent degradation since the samples were not analyzed immediately. Samples were subsequently stored in the refrigerator at 4 °C until analysis. All samples were filtered through a PTFE membrane with a pore size of 0.45 μm to remove suspended solids. Estrogens from these samples were then pre-concentrated using solid phase extraction (SPE) as described in **section S 4.0** in the supporting document.

2.10. Reuse efficiency

The reusability and durability of the most efficient nanocomposite photocatalyst, Fe@PSK@GO, was evaluated under the following experimental conditions. Photocatalyst dose: 0.02 g/L; steroid estrogen concentration: 5 mg/L; reaction time: 720 min; steroid estrogen solution: 30 mL. The experiment was carried out three times under the same conditions by using the same nanocomposite photocatalyst used in the previous experiment. After each experiment, the nanocomposite was recovered, rinsed with Millipore water, and dried in the oven at 60 °C for 5 h before reuse. All analysis of samples were carried out in triplicate.

3. Results and discussion

3.1. Photocatalyst characterization

Fig. 2A shows Raman spectra of Fe@PSK, GO, Fe@PSK@GO, *N*-Fe@PSK, and *N*-Fe@PSK@GO nanocomposites. The spectra show two bands near 1350 and 1600 cm^{-1}, known in the literature as D- and G-bands, respectively. The D band indicates disorder in GO originating from defects associated with vacancies, grain boundaries and amorphous carbon species, while the G band is attributed to the E_{2g} phonon of sp^2 C atoms in a 2-dimensional hexagonal lattice [35]. The D bands appear at 1350, 1352, 1347 and 1345 cm^{-1} for Fe@PSK, GO, Fe@PSK@GO, *N*-Fe@PSK and *N*-Fe@PSK@GO nanocomposites, respectively. This variability is consistent with chemical interactions between Fe@PSK, GO and APTES in the composites.

In contrast, the G band, which is generally stronger in the current spectra, always appears at 1598 cm^{-1}.

The attenuated total reflectance Fourier transform infrared (ATR-FTIR) analysis (Fig. 2B) of Fe@PSK, GO, Fe@PSK@GO, *N*-Fe@PSK, and *N*-Fe@PSK@GO nanocomposites was done to confirm the chemical functionalities present in these composites. The prepared GO material shows bands at 1724, 1622, 1400, 1219, 1383 and 1055 cm^{-1} assigned to CO and O = CO═— vibrations of carboxyl groups, C—OC— vibrations of epoxy groups along with C—O, CC═ stretch vibrations and the C—O band, respectively [36,37].

Moreover, all spectra show a broad peak centered around 3269 cm^{-1} that denotes the stretching vibration of −OH. This band is broad and intense in GO and all GO-modified nanocomposites. The peak at 1624 cm^{-1} in all the samples except GO is indicative of the presence of C═O stretching from amide groups [38]. However, this peak in GO sample is due to the stretching vibrations of C═C or unoxidized graphitic domains in GO [39] with a shoulder peak attributed to C ═O group [39]. The peak at 1020 cm^{-1} in all samples except GO

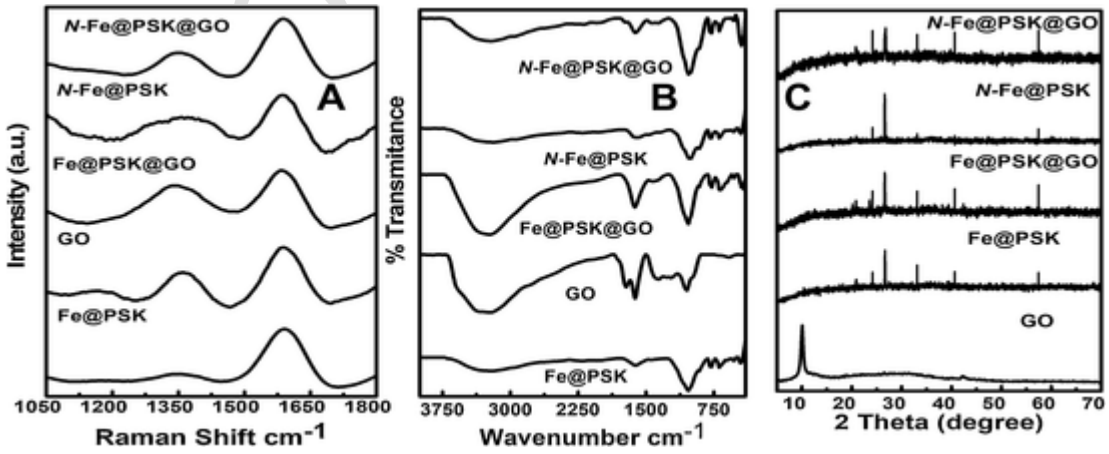

Fig. 2. (A) Raman spectra (B) Attenuated total reflectance-FTIR (C) X-ray diffraction pattern of prepared visible-light photocatalytic nanocomposites Fe@PSK, GO, Fe@PSK@GO, *N*-Fe@PSK and *N*-FeO@PSK @GO, respectively.

suggests the presence of Si-O-Si [40] in the nanocomposites. Furthermore, all spectra show bands at 1611 (−OH), 1031 (Si-O), 910 (Al−OH), 783 (diagnostic band for quartz), 664 (Al-Fe−OH), and 525 (Zn-O) cm^{-1} [41–43].

The X-ray diffraction (XRD, Fig. 2C) shows the characteristic graphene oxide peak at 2θ = 10.1° [44], the presence of kaolinite at 2θ = 20.3 (110) and 24.9° (002) and the characteristic quartz peak at 26.4° [45]. The reflections at 2θ = 23.8 (012), 32.8 (104), 40.3° (113) arise from hematite (ICSD 201,096). Further confirmation for the presence of Fe in the nanocomposites can be found from X-ray fluorescence spectroscopy **(Table S1, SI)**. Judging from XRD patterns, no new crystal phase was formed in the process of developing the nanocomposites. This suggests that modification of the nanocomposites were mere surface modification.

Electron paramagnetic resonance (EPR) spectra of the nanocomposites at 77 K (**see Fig. S1, SI document**) show a sharp signals at g = 2.01, a broader signal component with g near 2.63, and a weak signal at g = 4.34 for nanocomposites without GO. While the sharp signal most likely arises from organic free radicals left behind after the pyrolysis of the biomass, the other signals show the typical signature of high-spin Fe^{3+} species in hematite and various siliceous inorganic matrices. Spectra of this kind and their suggestions for their interpretation assignments have been extensively discussed in the literature [46–48], and are beyond the scope of this study. **Fig. S1** indicates that the spectroscopic variations for the present Fe-containing samples are insignificant, confirming that the nature of the iron species are unchanged by both the addition of GO and the surface modification with APTES.

Table 2
Brunauer-Emmett-Teller (BET) surface area, pore volume and pore size of the prepared photocatalytic composite.

Composite	Surface Area (m^2/g)	Pore Volume (cm^3/g)	Pore Size (Å)
Fe@PSK	189.8	0.208	22.1
N-Fe@PSK	59.8	0.074	24.8
Fe@PSK@GO	233.8	0.281	24.1
N-Fe@PSK@GO	125.8	0.171	27.2

The four composite materials show type IV nitrogen sorption isotherms [1] typical of porous materials **(Fig. S2, SI document**), and indeed, the pore sizes calculated from that data are in the microporous range **(**Table 2**)**. Moreover, the adsorption-desorption loop is a H3 loop; this may be related to the presence of slit-shaped pores [1,49]. The presence of APTES in the synthesis procedure significantly decrease the surface area of the prepared nanocomposites (Table 2).

The field emission scanning electron microscopy (FE-SEM) images of the nanocomposites show agglomerated materials with rough surfaces. The typical scale-like structure of GO is visible in the GO-modified nanocomposites **(**Fig. 3**A–E)**. This further confirms the successful incorporation of the GO into the composites, consistent with IR and Raman spectroscopy **(**Fig. 2**A-B)**.

Complementary high-resolution transmission electron microscopy (HR-TEM) images of Fe@PSK nanocomposite (**Fig. S3A, SI document**) shows rhombohedral Fe_2O_3 particles distributed on the surface of Fe@PSK nanocomposite. In contrast all other materials show much smaller particles distributed on a light gray but crumpled and folded background (the GO) **(Fig. S3B-D, SI document)**. All composites are different from kaolinite which show typical plate-like structures **(Fig. S3E, SI document)**. The selected area electron diffraction (SAED), pattern for the nanocomposites show that only the Fe@PSK nanocomposite show some level of crystallinity, similar to kaolinite **(Fig. S4, SI document).** The other nanocomposites are more amorphous than crystalline. However, the presence of APTES is seen to decrease the crystallinity of the nanocomposites and with the addition of GO, the nanocomposites lose more of their crystallinity **(Fig. S4, SI document)**.

X-ray photoelectron spectroscopy (XPS) analysis of Fe@PSK@GO nanocomposite (Fig. 4A) confirmed that it contains Fe, O, C, N, Si and Zn which agrees well with the elemental mapping result (Fig. S5). The binding energies peak at 284.2 and 286.2 eV confirm the presence of sp^3C of C—C and CO═ in Fe@PSK@GO nanocomposite (Fig. 4B) and the peak at 531.03 eV corresponds to O 1s chemical state (Fig. 4**B-C**) [50]. The auger electron for oxygen is seen at 974 eV [51]. These are all due to the presence of the organic component from the biomass and graphene oxide [52,53]. The complex multiple splitting peak and de-convoluted peaks at 710.7, and 724.7 eV (Fig. 4D) confirms the presence of Fe $2p_{3/2}$ and Fe $2p_{1/2}$ lines with their associated satellite peaks at 718 and 732.6 eV (Fig. 4D) respectively due to charge transference

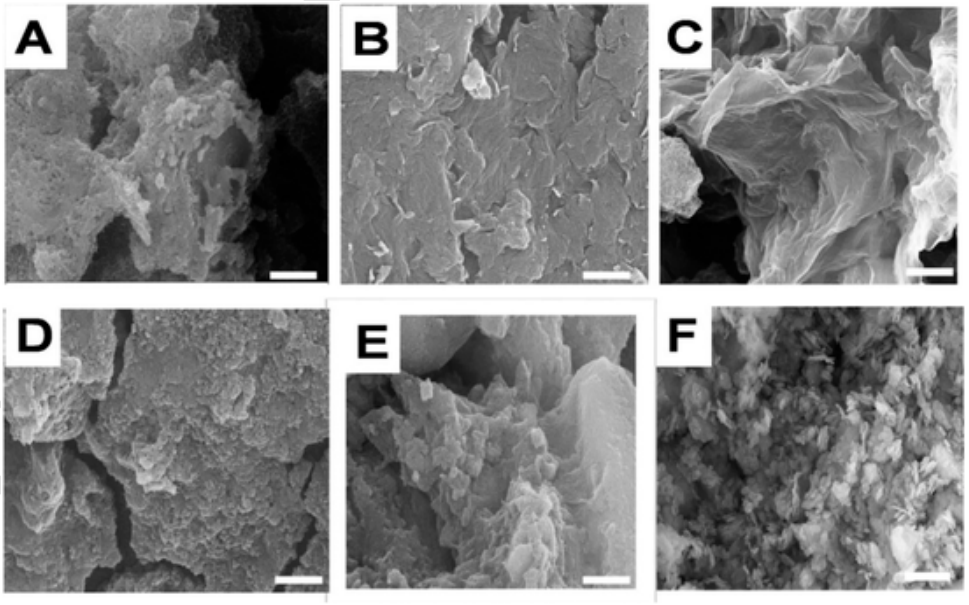

Fig. 3. Field Emission-Scanning Electron Microscopy images of (A) Fe@PSK (B) GO (C) Fe@PSK@GO (D) *N*-Fe@PSK (E) *N*-Fe@PSK@GO nanocomposites (F) kaolinite (All scale bar A-E =200 nm, F = 2 μm).

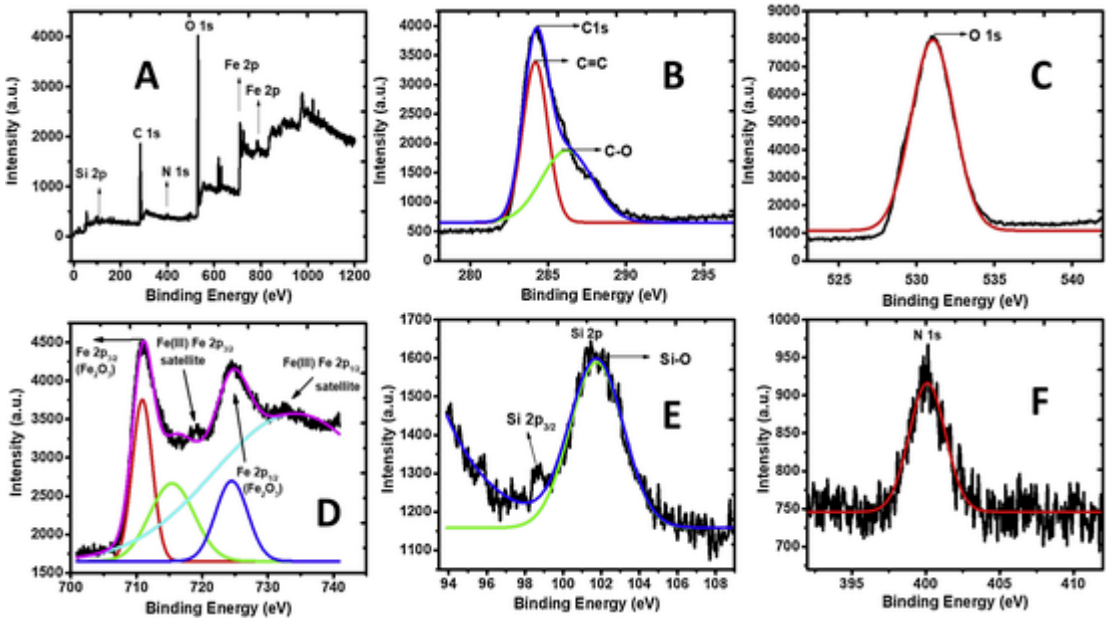

Fig. 4. (A) X-ray photoelectron spectroscopy (XPS) spectrum, (B) C 1s spectrum, (C) O 1s spectrum, (D) Fe 2p spectrum, (E) Si 2p spectrum and (F) N 1s spectrum of Fe@PSK@GO nanocomposite.

processes [54,55]. This corroborates our earlier results from XRD and IR analysis suggesting the presence of Fe_2O_3 in the nanocomposite. A low intensity peak at 400.1 eV (Fig. 4F) confirms N 1s in Si chemical environment [56] suggesting the presence of amine groups from *carica papaya* seeds which is known to contain nitrogenous compounds [57]. The peak at 101.8 eV indicate oxide phase of Si in an environment of C with an Si 2p 3/2 peak with very low intensity (Fig. 4E). In addition, there are Zn $2p^{1/2}$ and Zn $2p^{3/2}$ chemical states of Zn in ZnO in the Fe@PSK@GO nanocomposite which are found at 1022 and 1044.7 eV [58].

The thermal stability of the nanocomposites was characterized *via* thermogravimetric analysis (TGA) and the derivative loss (DTG) as shown in (Fig. 5). The Fe@PSK and *N*-Fe@PSK nanocomposites showed weight loss in three regions between 31 and 594 °C representing the elimination of physiosorbed or adsorbed water in the interlayer spaces at the edge and external surface of the composites (31–110 °C), volatilization 110–430 °C), and dehydroxylation of kaolinite (>430 °C) in the nanocomposites respectively [59,60]. However, for *N*-Fe@PSK

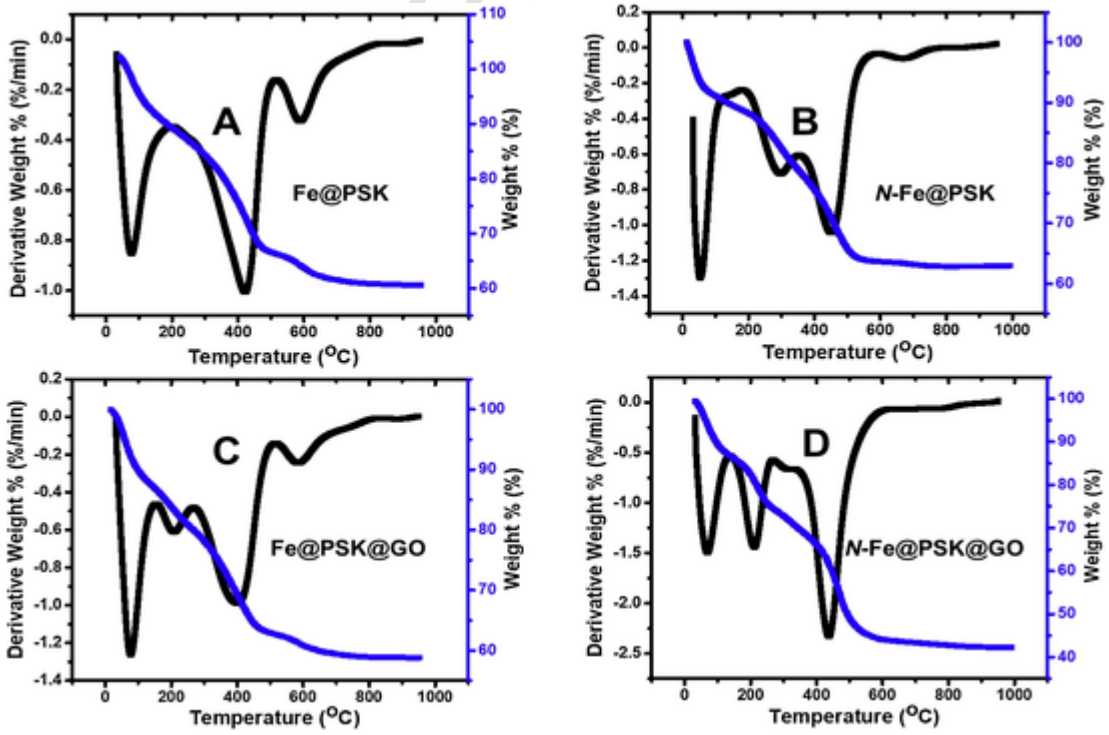

Fig. 5. Thermal gravimetric analysis (TGA) and derivative thermogravimetry (DTG) plots of (A) Fe@PSK, (B) Fe@PSK@GO, (C) *N*-Fe@PSK and (D) *N*-Fe@PSK@GO nanocomposites.

nanocomposite, there is a second loss of adsorbed water from the presence of APTES in the composite at 286 °C. Every weight loss is accompanied by the corresponding percentage derivative weight loss **(**Fig. 5**A-B).**

The GO-modified nanocomposites exhibit four regions of weight loss with their corresponding percentage derivative weight loss, which are linked to loss of absorbed water (31−110 °C), pyrolysis of GO (ca. 200 °C), loss of aliphatic groups (212−430 °C) and dehydroxylation of Kaolinite (>430 °C) [59–61]. The corresponding differential thermogram that supports these weight losses are seen at ca. 75, 210, 403 and 586 °C **(**Fig. 5**C-D)**. It should be noted that while the dehydroxylation of Kaolinite is pronounced in Fe@PSK and Fe@PSK@GO nanocomposites, it appears very weak in nanocomposites containing APTES. Furthermore, the *N*-Fe@PSK@GO sample show residual weight significantly lower (40 %) than in the other three samples. This supported by the Energy Dispersive X-ray data (**Table S2, SI document**) that suggest a higher carbon content in this sample than for others.

The optical absorbance properties of the nanocomposites were probed with UV-diffuse reflectance spectroscopy (UV-DRS) and photoluminescence spectroscopy (PL) **(**Fig. 6**)**. Fig. 6A shows absorbance plots for the nanocomposites with peaks at 288 nm. The indirect band gap fitting mode of the Tauc plot was used to determine the approximate apparent band gaps of Fe@PSK, *N*-Fe@PSK, Fe@PSK@GO and *N*-Fe@PSK@GO nanocomposites as 1.75, 1.86, 1.56 and 1.69, respectively (Fig. 6B**)**. It is suggested that the presence of carbon (from the biomass) and GO reduce band gap in materials [62].

The photoluminescence spectra of the same nanocomposites are as shown in Fig. 6C. At excitation wavelength of 288 nm, emission wavelengths for all nanocomposites are observed in the visible region **(**Fig. 6C**)** suggesting that these materials could be active as catalysts in the visible portion of the electromagnetic spectrum.

3.2. Photocatalytic-oxidation of steroid estrogens

To understand the influence of each component of the nanocomposites on the removal of steroid estrogens from water, a series of control experiments were carried out using experimental method described in section 2.5 except that samples were only withdrawn and analyzed for steroid estrogen after 720 min. Fig. 7 shows that the material without Fe or GO (N-K) exhibit removal efficiency of less than 5% while those with the GO, Fe and GO/Fe components showed expected higher efficiency between 20 and 56 %. Infact, most of these materials show less efficiency for the removal of these steroid estrogens from water than GO itself (Fig. 7A–D). The more considerable influence on photocatalytic efficiency is seen with the presence of carbon as seen in Fe@PSK@GO nanocomposite for all steroid estrogens (Fig. 7). This result suggests that carbonaceous species, arising from biomass oxidation, may be responsible for this effect, perhaps by decreasing electron-hole recombination rates [63,64]

It is important to state that kaolinite serves as a support base, and the hydrolysis of $ZnCl_2$, followed by calcination in the presence of biomass for Fe@PSK@GO nanocomposite creates a nanoporous and nanostructured material (as seen from its specific surface area Table 2 and it TEM images in Fig. S3, SI document), which is imparted with photocatalytic activity via precipitating it together with either graphene oxide, and/or nanocrystalline iron oxide. The role of the APTES modification is principally to introduce a heteroatom (nitrogen) which is exoected to increase photoactivity of the nanocomposite. Indeed, APTES modification reduced the effective surface area and pore volume, diminishing to some extent the photocatalytic performance of the material (Table 2 and Fig. 7).

Since photocatalytic processes consist of three concomitant steps (adsorption unto the photocatalyst surface, photolysis, and degradation), it is important to evaluate how these steps influence the photo-

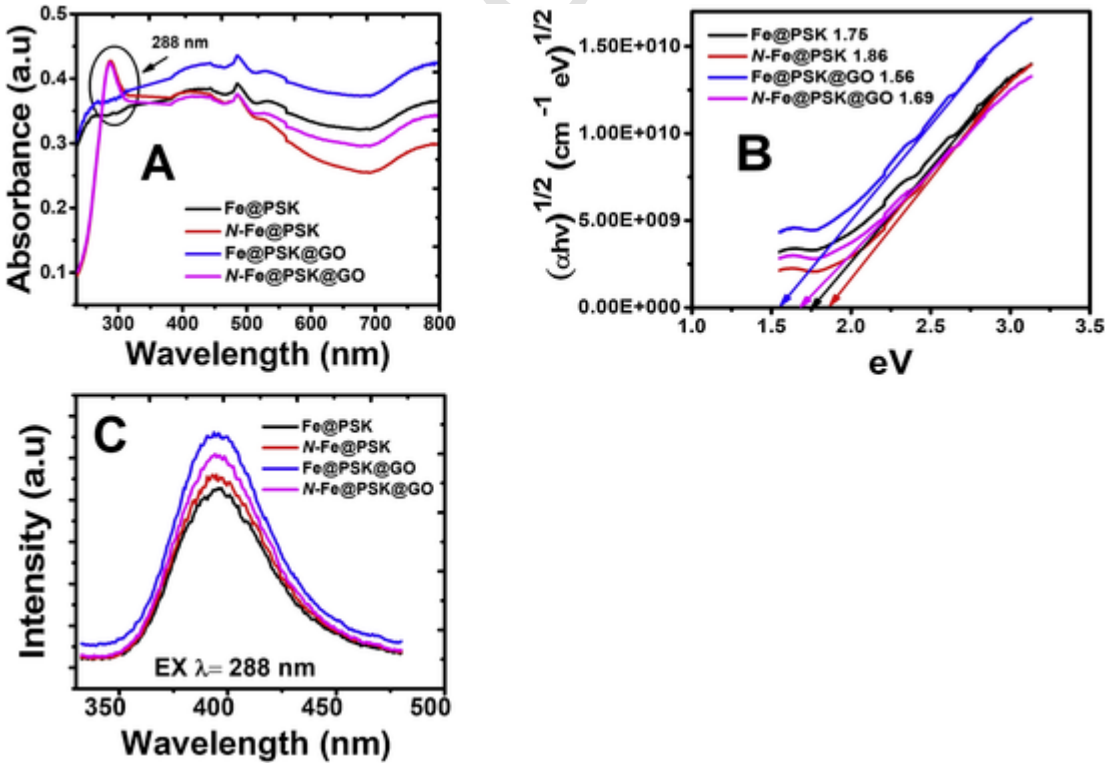

Fig. 6. (A) UV–vis diffuse reflectance spectroscopy (UV-DRS), (B) Tauc plot and (C) photoluminescence spectra at room temperature for Fe@PSK, Fe@PSK@GO, *N*-Fe@PSK, *N*-Fe@PSK@GO nanocomposites.

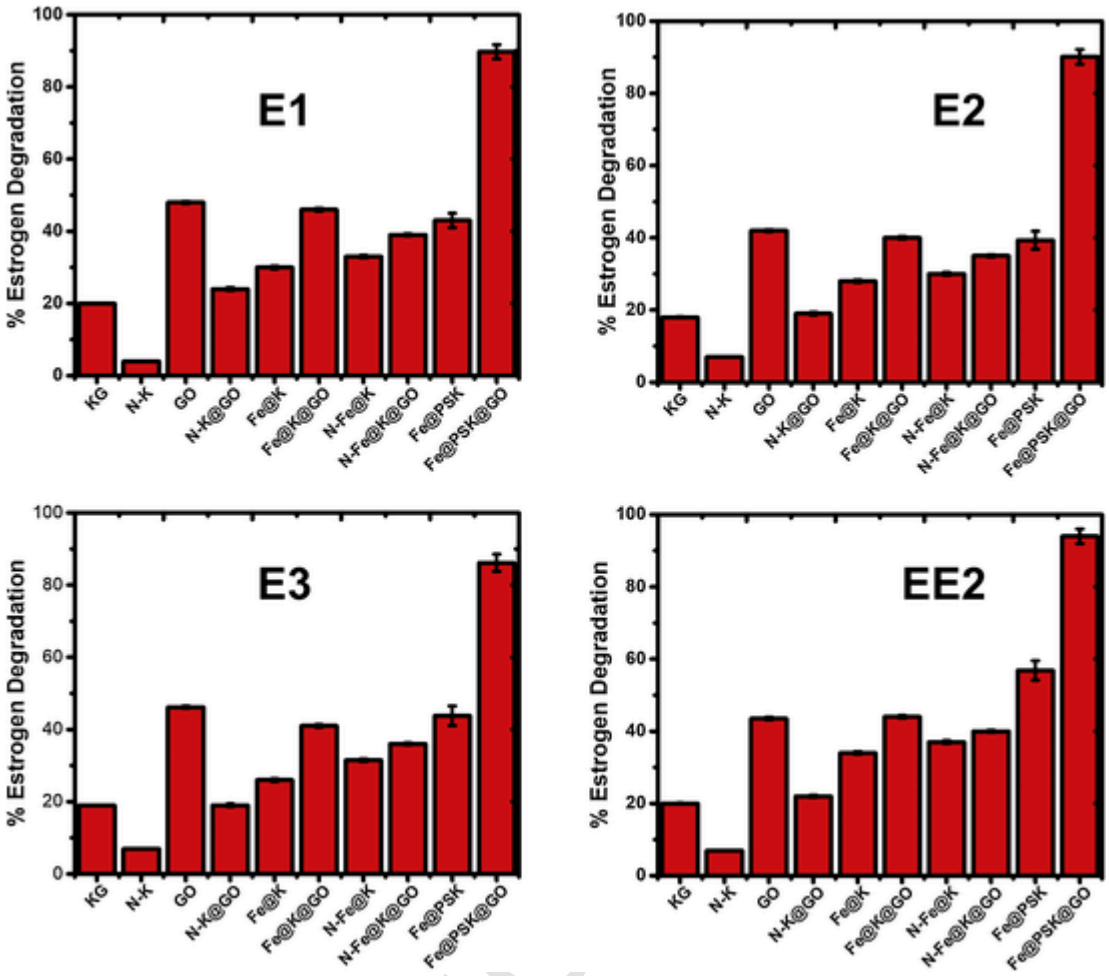

Fig. 7. Control experiments for the efficiency of each component of photocatalytic nanocomposite materials prepared.

catalytic degradation of the steroid hormones (E1, E2, E3, and EE2). To this end, a control experiment involving photolysis of the estrogens in the presence of visible-light in the absence of nanocomposite was used. The results clearly show that simple irradiation already leads to some degradation in all cases (via photolysis), but that the fraction of degraded estrogens is rather low: E1 (28 %), E2 (22 %), E3 (22 %), and EE2 (24 %) after 720 min of irradiation (Fig. 8 **A–D).**

To understand the influence of adsorption on estrogen removal, the nanocomposites were agitated in a solution of the estrogens in the dark for 720 min **(**Fig. 8 **E–H).** The results show an increased estrogen removal from water when compared with results from photolysis as a result of adsorption, suggesting that adsorption also contributes to estrogen removal from solution.

However, in the presence of visible light, the efficiencies of the nanocomposites in estrogen removal are further enhanced **(**Fig. 8 **E–H).** GO-modified nanocomposites consistently give the best results between ca. 89 and ca. 94 % of estrogen removal. This suggests that the nanocomposites are efficient adsorbents for the removal of estrogens but that the true benefit in the materials lies in the combination of adsorption and photocatalytic degradation of steroid estrogens. A simple estimation shows that, for example, E1 is degraded to about 28 % by photolysis only **(**Fig. 8A**)** and removed the estrogen from solution to about 35 % by adsorption on Fe@PSK@GO nanocomposite and photolysis as well **(**Fig. 8E**).** Irradiation of estrogen solutions in the presence of Fe@PSK@GO nanocomposite, however, leads to a significantly higher degree of estrogen removal of about 81 % **(**Fig. 8E**),** a >2-fold increase in the efficiency of the photocatalyst.

The degree of complete oxidation to carbon dioxide and water was investigated for the most efficient nanocomposite, Fe@PSK@GO. Fig. 8**I** shows that complete oxidation (conversion of the organic fraction to CO_2) is rather high and reaches its highest value for EE2 with slightly over 73 %.

The fact that the overall levels of complete oxidation is somewhat lower that the total percentage of estrogen removal supports the above statement that a certain fraction of the estrogens is indeed removed by adsorption and others could be transformation products.

To ascertain toxicity levels of treated and untreated water, based on the possible presence of these chemical intermediates in the water, an acute toxicity test was carried out following the standards by the Brazilian Association of Technical Standards [65]. **Fig. S6 A–D** (**SI document**) shows a clear dose-response relationship between *C. daphnia spp* and the steroid estrogens, since increasing steroid estrogen concentrations increased mortality. The ranking of relative toxicity (LC_{50} in mg/L) is E1 (7.69) ≈ E3 (7.70) < EE2 (6.71) < E2 (6.56). The lethal effects of these estrogens become significant above 6.50 mg/L (acute level). The results of the toxicity test for treated water effluents show no lethal influence on *C. daphnia spp* suggesting that the possible presence of intermediates in the treated water does not pose any health risk to humans.

Our kinetic studies **(Fig. S7, SI document)** indicate that the rate of photocatalytic oxidation follows a first-order kinetic model and that the reaction occurs at the solid-liquid interface. The results of this analysis are summarized in Table 3. Again, the Fe@PSK@GO nanocomposite shows the best photocatalytic performance, indicating that the intro-

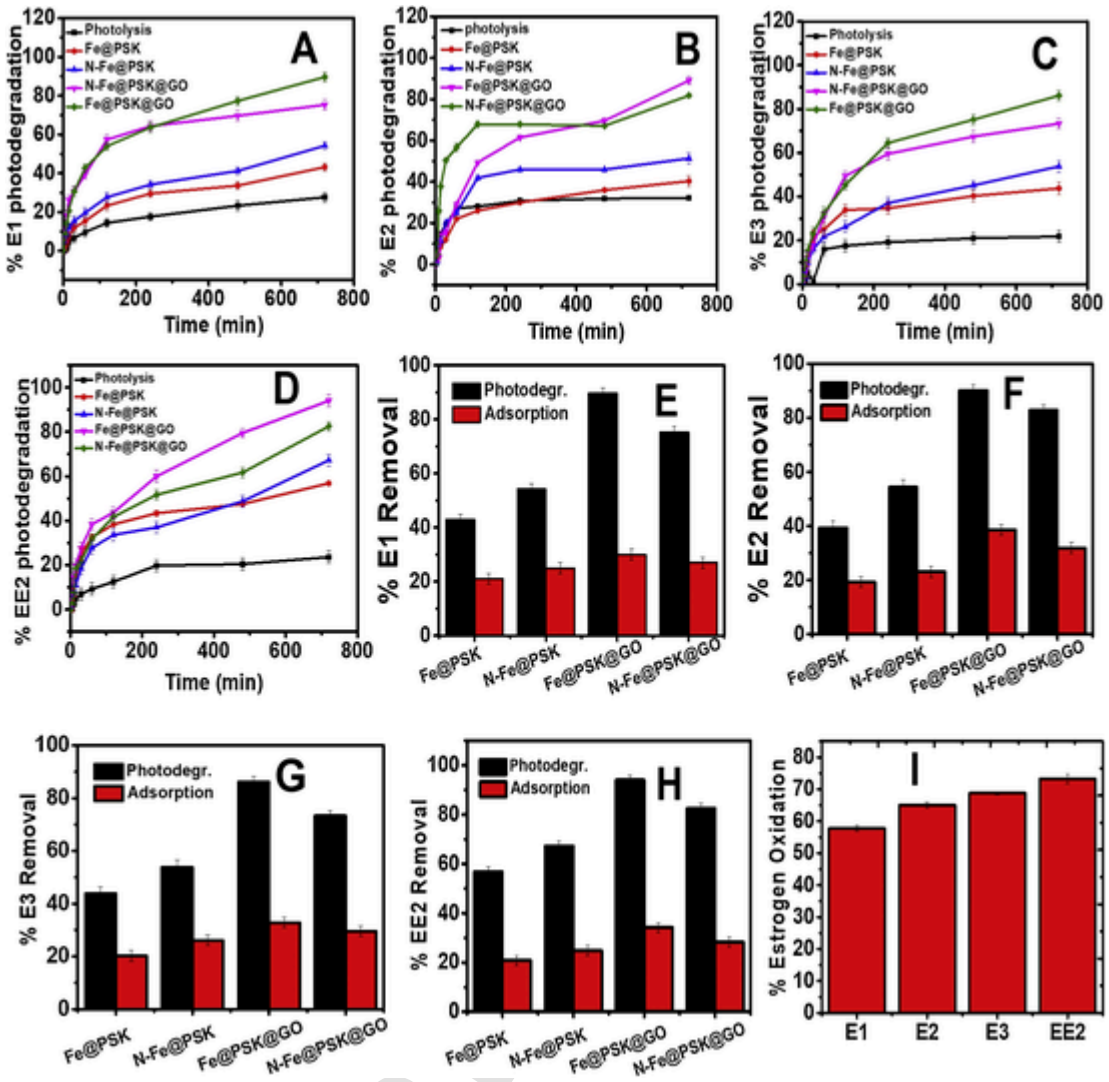

Fig. 8. Photolysis, adsorption, and photodegradation of (A, E) E1, (B, F) E2, (C, G) E3, and (D, H) EE2 steroid estrogens. (I) Fraction (%) of estrogens removed by Fe@PSK@GO nanocomposite. Black data points in A-D show degradation from pure photolysis (no composite present) vs. time. Colored datasets in A-D show effect of different composites on photodegradation. Figures E-H provides information on the influence of the various components of the nanocomposites and their various combination on the removal of steroid estrogens in water. The term "adsorption" in E-H refers to percentage of steroids removed by adsorption on the composites in the dark and "photodegradation" refers to the combined effect of adsorption and irradiation in the presence of composite.

duction of GO into the nanocomposite increases the rate of photocatalytic oxidation of steroid estrogens. The rates of photocatalytic oxidation of EE2 and E2 estrogens are greater than those for E3 and E1 estrogens. This trend was also seen by Coleman [66] using TiO_2 as photocatalyst. It is possible that the rapid photocatalytic degradation of EE2 is due to its low stability arising from the presence of the ethynyl group which absorbs light and is easily oxidized [9]. On the other hand, the addition of –OH groups may make the phenolic rings more stable, resulting in a considerable drop in the removal rate of E2 and a significant decrease for E3 [67].

In any case, the EE2 and E2 estrogens are the most potent among the four hormones discussed here while E3 has the lowest estrogenicity [67].

3.3. Influence of process variables

Certain process variables are required to be optimized to fully understand the operational limits for optimal performance of the photocatalyst. These variables include solution pH, photocatalyst dose, ionic strength, presence of anions, and initial concentration of steroid estrogens. The influence of these parameters was studied with the photocatalyst with the best efficiency for the estrogen removal, Fe@PSK@GO nanocomposite.

Fig. 9**A** shows that the efficiency of the photocatalytic oxidation increases as more catalyst is present in the mixture. Consistent with the data shown above (Fig. 7I), EE2 is degraded most effectively. Likely, this increased efficiency vs. increasing weight is related to an increasing number of the available active catalytic sites [32,68]. It must be noted however, that the photocatalytic oxidation efficiency decreases again at catalyst loadings of 0.17–1.67 g/L. This is because catalyst loadings above lead to turbid dispersions and agglomeration reducing both the number of available catalytic cycles and the light intensity on the catalyst [69].

Fig. 9**B** shows that the initial concentration of the estrogens correlates with photodegradation efficiency. Likely, the decline in efficiency with increasing concentration is associated with the fact that at higher estrogen concentrations the number of catalytically active sites available is not sufficient to degrade all molecules. Moreover, some of the sites may be inactivated by adsorption of some estrogen molecules.

Table 3
Kinetic parameters for the photocatalytic oxidation of steroid estrogens with Fe@PSK, Fe@PSK@GO, *N*-Fe@PSK, and *N*-Fe@PSK@GO photocatalytic nanocomposites.

E1			
PHOTOCATALYST	k_{app} (min $^{-1}$)	$t_{1/2}$ (min)	;r2
Fe@PSK	0.0017	239.6	0.9742
N-Fe@PSK	0.0039	178.2	0.9261
Fe@PSK@GO	0.0060	112.1	0.9902
N-Fe@PSK @GO	0.0043	158.5	0.9896
E2			
PHOTOCATALYST	k_{app} (min $^{-1}$)	$t_{1/2}$ (min)	;r2
Fe@PSK	0.0042	172.4	0.9622
N-Fe@PSK	0.0049	146.8	0.8924
Fe@PSK@GO	0.0063	120.0	0.9012
N-Fe@PSK @GO	0.0050	136.4	0.9428
E3			
PHOTOCATALYST	k_{app} (min $^{-1}$)	$t_{1/2}$ (min)	;r2
Fe@PSK	0.0023	145.2	0.9742
N-Fe@PSK	0.0045	153.9	0.9228
Fe@PSK@GO	0.0053	196.8	0.9821
N-Fe@PSK@GO	0.0042	170.4	0.8999
EE2			
PHOTOCATALYST	k_{app} (min $^{-1}$)	$t_{1/2}$ (min)	;r2
Fe@PSK	0.0048	152.2	0.9712
N-Fe@PSK	0.0057	124.4	0.9962
Fe@PSK@GO	0.0068	105.2	0.9982
N-Fe@PSK@GO	0.0059	130.8	0.8241

Fig. 9**C** shows that the ionic strength of the estrogen solution using different concentrations of NaCl (a common electrolyte in drinking water) does not significantly influence the photodegradation efficiency of Fe@PSK@GO nanocomposite. The efficiency remains at >80 % irrespective of the electrolyte concentration or estrogen type. This is different from a previous report on the adsorption of E2 onto GO suggesting an increase in the adsorption efficiency of GO [26] with an increase in ionic strength. Overall, however, there is a dearth of data on the influence of ionic strength on the photocatalytic removal of estrogens from water under visible-light conditions so at the moment a final conclusion on these effects is difficult.

Fig. 9**D** shows the effects of pH. The highest removal efficiencies are observed at pH 6.0, with EE2 being removed the best. Above pH 6.0, the efficiency of the photocatalyst is lower and keeps decreasing with increasing pH. The pH of solution is known to influence the surface charge of material as well as the dissociation properties of organic contaminants. Even though we expect the surface charge of Fe@PSK@GO photocatalytic nanocomposite to be negatively charged above its pHpzc of 4.2 **(Fig. S8, SI document)** in estrogen solution of pH 7.3, yet the electrostatic theory will not be able to explain the trend of results shown in Fig. 9D especially because the pKa of these estrogens is ca. 10.4 [67]. Hydrophobic interaction, hydrogen bonding and dissociation properties is postulated to explain the trend. When the initial pH of aqueous solution is less than 9.0, the dissociation of the estrogen molecules (pKa ≈10.4) is partially suppressed, causing them to exist in their non-dissociated form. Therefore, even though the electrical charge of the photocatalyst gradually changes from positive to negative (when pH exceeded 4.2), electrostatic repulsion would not be the major force of interaction. In this case, it will be hydrogen bonding between the hydroxyl of the estrogens and nitrogen and/or oxygen atoms on the surface of the photocatalyst [70]. Another important factor that could possibly affect the adsorption of the estrogen is hydrophobic interaction wherein the hydrophobic phase in the interlayer region of the photocatalyst is expected to interact with the estrogens via π-π interaction. As pH of the estrogen solution exceeds from 8.0, the increased hydroxyl ion could result in repulsive electrostatic interactions leading to a further decline in the efficiency of the photocatalyst to remove these estrogens from water [70].

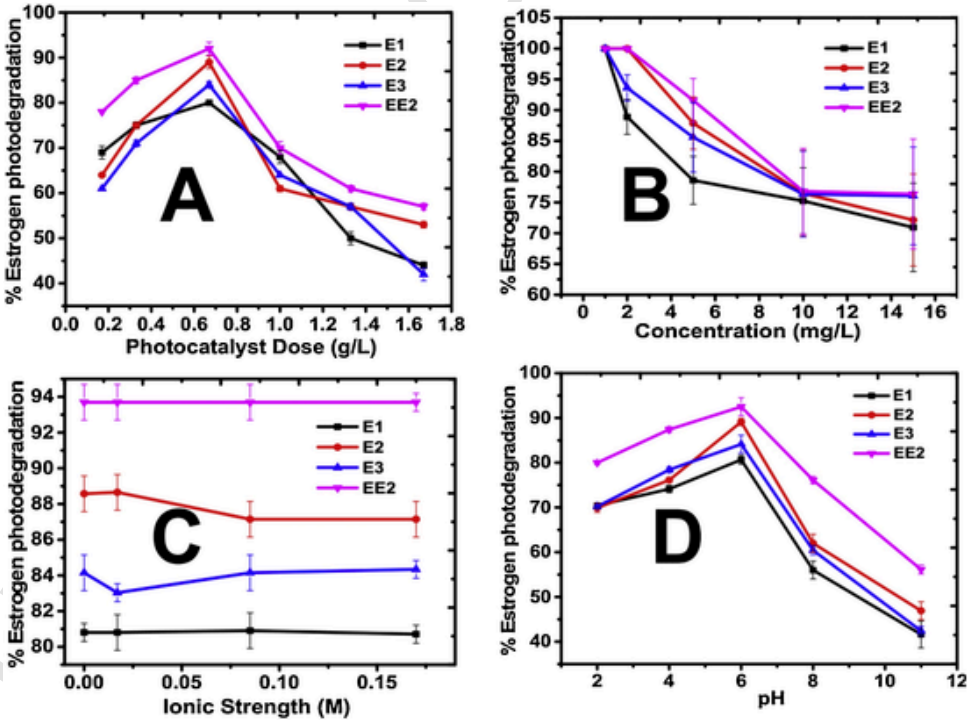

Fig. 9. Effect of process parameters on estrogen photodegradation. (A) Photodegradation vs. catalyst dose (0.17, 0.33, 0.67, 1.0, 1.33, 1.67 g/L) for initial estrogen concentration of 5 mg/L. (B) Photodegradation vs. initial steroid estrogen concentration using a photocatalyst dose of 0.67 g/L. (C) Photodegradation vs. ionic strength with photocatalyst concentration of 0.67 g/L and steroid concentration of 5 mg/L. (D) Photodegradation vs. initial solution pH with photocatalyst concentration of 0.67 g/L and steroid concentration of 5 mg/L. Photocatalyst is Fe@PSK@GO nanocomposite in all experiments.

In any case, these results support our earlier conclusion that adsorption is one of the mechanisms for the removal of these estrogen molecules from water using the Fe@PSK@GO photocatalytic nanocomposite. However, our results differ from those obtained with TiO_2 suspensions for the photocatalytic removal of E2 where a continuous decline in efficiency from pH 2.0 till pH 9.0 was noted [71].

Fig. 10 shows the effects of inorganic anions on the performance of the composites. Inorganic anions are important because they are common in drinking water. A small decrease in the photocatalytic efficiency was observed in the presence of sulphate while bicarbonate and phosphate leads to more drastic reductions. One possible explanation for this difference between sulfate and the other ions could be that bicarbonate and phosphate ions are efficient ·OH radical scavengers [72]. Some other report suggests that their presence increase the rate of h^+ oxidation which reduces the overall efficiency of the photocatalyst. This hole (h^+) oxidation is shown to be more in the presence of phosphate than in carbonate [72]. Given the result in Fig. 10, it is plausible to attribute the significant decrease in the efficiency of Fe@PSK@GO photocatalytic nanocomposite observed here, to hole (h^+) oxidation by these anions (phosphate and carbonate). This is an indication that the photocatalytic function of the nanocomposite is based on hole (h^+) generation. The results shown in Fig. 10 indicate a need for the initial removal of these anions via an anion exchange resin or other suitable techniques.

To ascertain the kind of reactive species produced by Fe@PSK@GO nanocomposite, the formation of hydroxyl radicals (·OH), superoxide radicals ($\cdot O_2^-$), and holes (h^+) were investigated by introducing propanol (IPA), benzoquinone (BQ), and ammonium oxalate (AO) scavengers, respectively, into the solutions containing a mixture of steroid estrogens and Fe@PSK@GO nanocomposite (see section 2.8). Fig. 11 shows that the addition of scavengers does reduce the efficiency of Fe@PSK@GO nanocomposite to photo-oxidize. The strong effect of BQ and AO radical scavengers on the photocatalytic oxidation efficiency of Fe@PSK@GO nanocomposite is more profound than that of IPA. Moreover, the strongest effect is seen when E1 is present. This presumes that the composite produces more superoxide radicals ($O_2^{\bullet-}$) and hole (h^+) reactive species than the hydroxyl radicals (·OH) in solution when exposed to visible-light and in water. Fig. 11 therefore, suggests that the most reactive species h^+, followed by ($\cdot O_2^-$) and finally ·OH.

The strong negative influence of BQ and AO radical scavengers on the photocatalytic oxidation efficiency of Fe@PSK@GO nanocomposite is more pronounced than that of IPA, and even so, this influence is more with E1 estrogen **(**Fig. 11**)** than with the other estrogens. This presumes that the composite produces more superoxide radicals ($\cdot O_2^-$) and hole (h^+) reactive species than the hydroxyl radicals (HO·) in solution when exposed to visible-light and in water. With respect to the results obtained in Fig. 11, the order of significance of reactive radicals produced by the composite is $h^+ > \cdot O_2^- >$ HO·.

Scheme 1 shows the tentative reaction mechanism of Fe@PSK@GO photocatalytic nanocomposite leading to the release of reactive oxygen species responsible for degradation of steroid estrogens. The theoretical band edge for both Fe_2O_3 have been calculated to be 2.4 eV and 0.3 eV [73] while that for graphene oxide (GO) is 3.4 eV and -0.51 eV [74]

The reactive species (superoxide radicals and holes) can react with H_2O to form hydroxyl radicals (HO·) which then interacts with estrogens to form CO_2, H_2O and transformed products (scheme 1).

$$E + \cdot O_2^-/\cdot OH \rightarrow E * \text{product} \quad (4)$$

Where E denotes the estrogen and $E^*_{product}$ is the photo-oxidized product of estrogen.

In addition, the GO component and *carica papaya* seeds into the composite does decrease the high recombination rate of e^-/h^+ in Fe_2O_3 [75,76], increasing the photocatalytic oxidation efficiency of the nanocomposite material. To confirm this, there is increase in photocatalytic efficiency from 28 to 33% with Fe@K material **(**Fig. 7**)** to 39–57 % when carbon was introduced to the Fe@K (Fe@PSK) as shown in Fig. 8E–H. This efficiency was further extended to 80–90% when GO included in Fe@PSK [Fe@PSK@GO] **(**Fig. 8**E–H).**

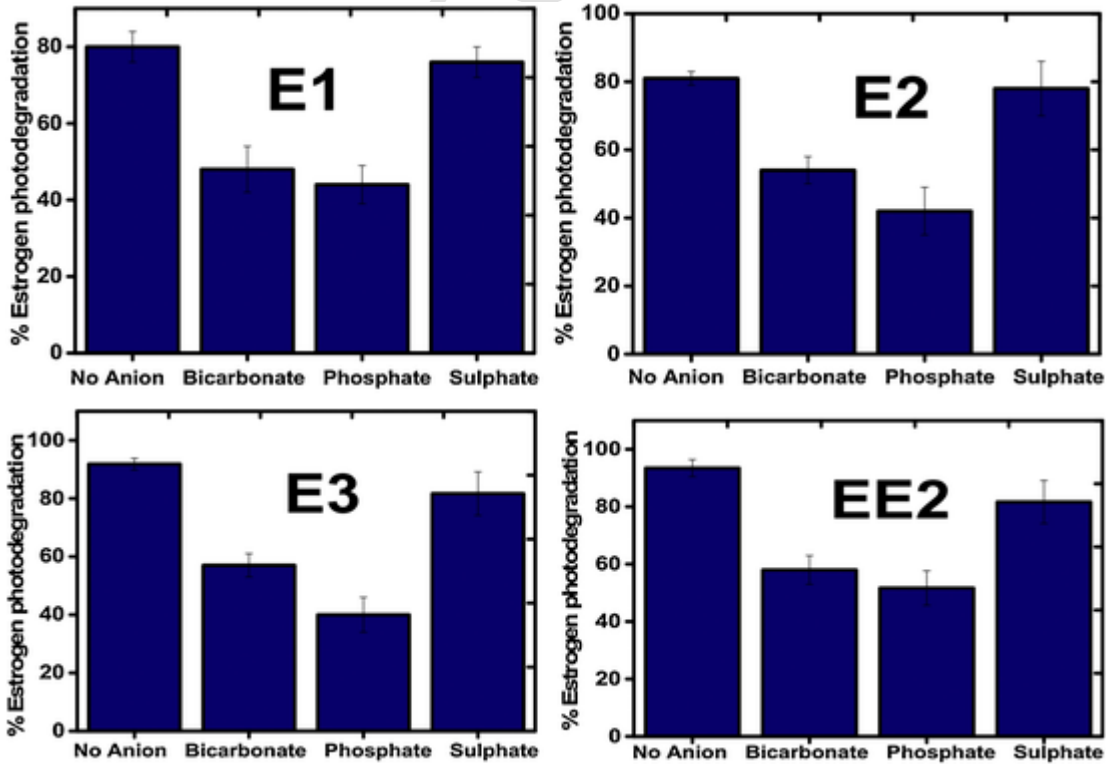

Fig. 10. Effect of Anions on Photo-oxidation of Steroids Estrogens using Fe@PSK@GO nanocomposite.

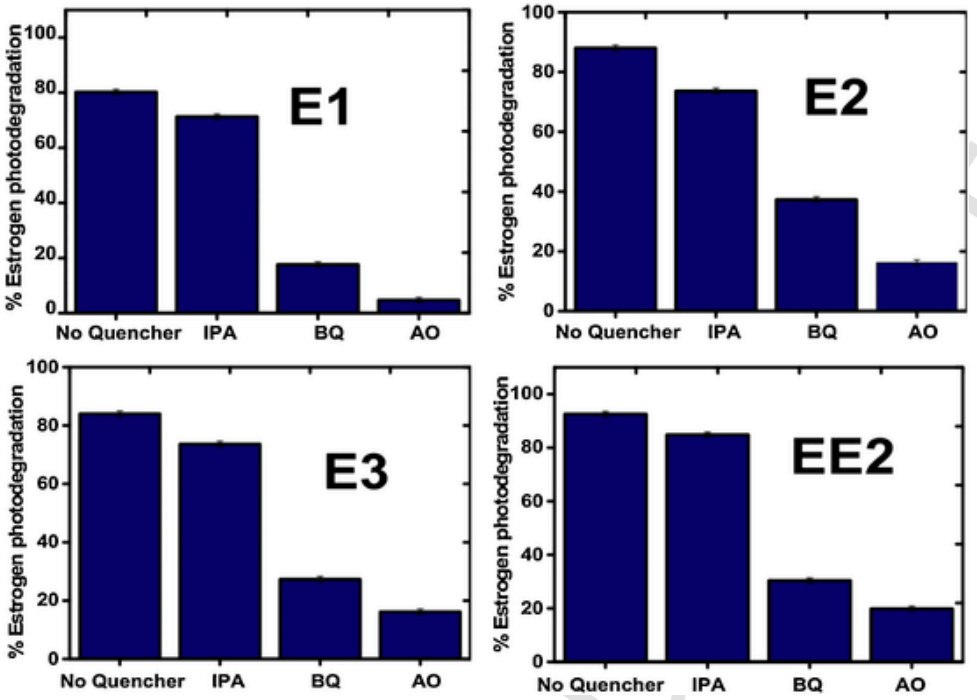

Fig. 11. The effect of scavengers (propanol - IPA, benzoquinone – BQ, and ammonium oxalate – AO) on the efficiency of Fe@PSK@GO nanocomposite for estrogen photodegradation.

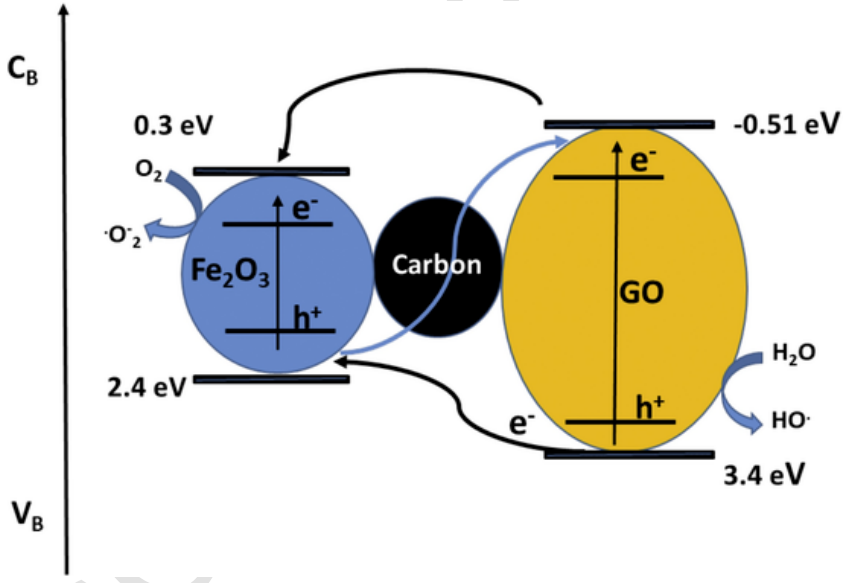

Scheme 1. Generation of Reactive Oxygen Species by Fe@PSK@GO nanocomposite (C_B and V_B).

3.3.1. Treatment of raw wastewater and drinking water

To determine the efficiency of Fe@PSK@GO nanocomposite for estrogen removal from raw wastewater, tap water, and rainwater, these matrices were spiked with 10 mg L^{-1} of each of the estrogen. Millipore water is used as the control and was spiked with the same concentration of the estrogens. **Table S3 (SI document)** shows some basic physicochemical properties of the various water matrices. Table 4 shows that only the wastewater matrix contains a measurable amount of estrogens prior to spiking. This is because contraceptives (birth control pills) are massively used globally; they contain EE2 and are often excreted and transported into the central municipal wastewater systems. Table 4 shows that the levels of estrogen removal follows the se-

Table 4
Levels of removal of steroid estrogens from Millipore water, Rainwater, Tap water and Wastewater samples using Fe@PSK@GO nanocomposite.

	Removal of E1 %	Removal of E2 %	Removal of E3 %	Removal of EE2 %
Millipore water	81 (ND)	89 (ND)	84 (ND)	93 (ND)
Rainwater	77 (ND)	84 (ND)	77 (ND)	91 (ND)
Tap water	75 (ND)	79 (ND)	79 (ND)	89 (ND)
Wastewater	66 (0.42)*	67 (0.38)*	63 (0.40)*	78 (0.59)*

ND = Not detected.
* Values in bracket are the initial concentrations of the estrogens (mg/L) before spiking.

quence: Millipore water (control) > rain water > tap water > wastewater.

Clearly however, Table 4 also shows that there is a significant reduction in the efficiency of Fe@PSK@GO in "real" systems with the most challenging matrix being the wastewater matrix. Likely, some other solutes (other than the estrogens) compete for active sites on the photocatalytic nanocomposite and reactive species present in the reaction medium. In any case, the Fe@PSK@GO nanocomposite holds significant potential for the treatment of real wastewater systems containing these (and possibly related) steroid estrogens.

3.3.2. Competitive degradation of the steroid estrogens

To evaluate the efficiency of the photocatalyst in the presence of multiple estrogens at different concentrations, a test system with all estrogens (E1 = 100 μg/L, E2 = 100 μg/L, E3 = 100 μg/L, EE2 = 200 μg/L) was studied. The estrogen concentrations are such that they represent their relative concentration in environmental matrices, i.e., the concentration of EE2 is usually higher than the other three steroids (even though a previous study cites E1 as more abundant in the environment [77]).

Fig. 12**A** shows that the steroids are degraded effectively also when present as a mixture. The order of degradation is EE2 > E2 > E1 > E3 with the percentage of removal being 93, 89, 84, and 82 %, respectively. A similar order has been observed in Frontistis et al. [77]. Aside from that article, the current study is one of the first reports on the use of heterogeneous photocatalyst for visible-light oxidation of estrogens in a competitive system simultaneously in water. Other reports have reported on the use of harsher methods such as UV-light [22], potassium permanganate [78], UV/H_2O_2 [27], or potassium permanganate combined with ultrasound [79].

3.3.3. Reuse efficiency

Finally, the reuse efficiency and stability of Fe@PSK@GO nanocomposite was evaluated. Fig. 12**B** shows that the catalyst is stable at least for three cycles and does not significantly lose efficiency over the three-cycle test period. Clearly, there is a need for longer test phases but these initial data are quite promising.

4. Conclusion

The synthesis of low cost-high performance water treatment materials is a tremendous challenge, in particular for endocrine disruptors, which are only present in low concentrations in aqueous media. Here we report a group of new and highly promising candidates for removal of steroid estrogens from water. Nanocomposites containing graphene oxide (GO) are superior in their photocatalytic activities over those without GO. While the mechanism of the photocatalyst is not entirely clear, the most promising material, Fe@PSK@GO nanocomposite, clearly holds potential for the treatment of wastewater or other waters in real systems. The key findings of the study are that (1) the materials also work with mixtures of steroids and keep their efficiency over at least three cycles, (2) the treated water samples show no toxicity towards *Cerio daphnia silvestrii spp*, and (3) there is no need to use UV light for successful application of the catalyst. Overall, the materials and processes introduced here are highly potent materials with high application potential in wastewater treatment, in particular for steroid removal.

Declaration of Competing Interest

The authors declare that they have no known competing financial interests or personal relationships that could have appeared to influence the work reported in this paper.

Acknowledgement

Bayode Ajibola Abiodun expresses her thanks to the African-German Network of Excellence in Science (AGNES) for granting a Mobility Grant in 2018. The grant is generously sponsored by German Federal Ministry of Education and Research and supported by the Alexander von Humboldt Foundation. This research is also supported by The World Academy of Sciences- Brazilian National Council for Scientific and Technological Development (TWAS-CNPq) award number 315710/2018-7 and the fund from FAPESP: 2018/16244-0.

Appendix A. Supplementary data

Supplementary material related to this article can be found, in the online version, at doi:https://doi.org/10.1016/j.jwpe.2020.101865.

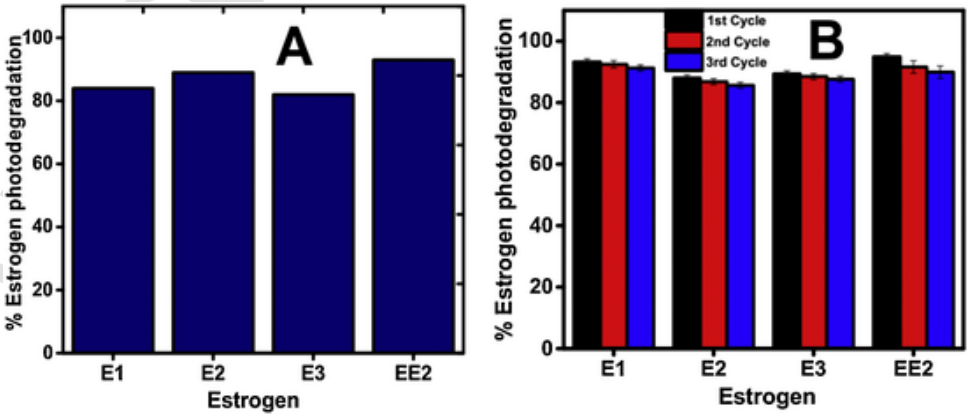

Fig. 12. (A) Competitive photodegradation of steroid estrogens from a steroid mixture using Fe@PSK@GO. (B) Estrogen photodegradation in three reuse cycles.

References

Liu, S., Liu, Y., Jiang, L., Zeng, G., Li, Y., Zeng, Z., Wang, X., Ning, Q., 2019. Removal of 17β-Estradiol from water by adsorption onto montmorillonite-carbon hybrids derived from pyrolysis carbonization of carboxymethyl cellulose. J. Environ. Manage. 236, 25–33.

Nikolaou, A., Meric, S., Fatta, D., 2007. Occurrence patterns of pharmaceuticals in water and wastewater environments. Anal. Bioanal. Chem. 387, 1225–1234.

Kabir, E.R., Rahman, M.S., Rahman, I., 2015. A review on endocrine disruptors and their possible impacts on human health. Environ. Toxicol. Pharmacol. 40, 241–258.

Westerhoff, P., Yoon, Y., Snyder, S., Wert, E., 2005. Fate of endocrine-disruptor, pharmaceutical, and personal care product chemicals during simulated drinking water treatment processes. Environ. Sci. Technol. 39, 6649–6663.

Rovani, S., Censi, M.T., Pedrotti, S.L., Jr., Lima, É.C., Cataluña, R., Fernandes, A.N., 2014. Development of a new adsorbent from agro-industrial waste and its potential use in endocrine disruptor compound removal. J. Hazard. Mater. 271, 311–320.

Sornalingam, K., McDonagh, A., Zhou, J.L., 2016. Photodegradation of estrogenic endocrine disrupting steroidal hormones in aqueous systems: progress and future challenges. Sci. Total Environ. 550, 209–224.

Sun, Y., Huang, H., Sun, Y., Wang, C., Shi, X.-L., Hu, H.-Y., Kameya, T., Fujie, K., 2013. Ecological risk of estrogenic endocrine disrupting chemicals in sewage plant effluent and reclaimed water. Environ. Pollut. 180, 339–344.

Ronan, J.M., McHugh, B., 2013. A sensitive liquid chromatography/tandem mass spectrometry method for the determination of natural and synthetic steroid estrogens in seawater and marine biota, with a focus on proposed Water Framework Directive Environmental Quality Standards. Rapid Commun. Mass Spectrom. 27, 738–746.

Zuo, Y., Zhang, K., Zhou, S., 2013. Determination of estrogenic steroids and microbial and photochemical degradation of 17α-ethinylestradiol (EE2) in lake surface water, a case study. Environ. Sci. Process. Impacts 15, 1529–1535.

Kuster, M., de Alda, M.J.L., Barceló, D., 2004. Analysis and distribution of estrogens and progestogens in sewage sludge, soils and sediments. Trac Trends Anal. Chem. 23, 790–798.

Adeel, M., Song, X., Wang, Y., Francis, D., Yang, Y., 2017. Environmental impact of estrogens on human, animal and plant life: a critical review. Environ. Int. 99, 107–119.

Huang, J., Liu, Y., Hou, H., You, T., 2008. Simultaneous electrochemical determination of dopamine, uric acid and ascorbic acid using palladium nanoparticle-loaded carbon nanofibers modified electrode. Biosens. Bioelectron. 24, 632–637.

Phuc Thuong, N., Sung, Y.Y., Ambak, M.A., Abol-Munafi, A.B., 2017. The hormone 17β-estradiol promotes feminization of juveniles protandrous hermaphrodite false clownfish (Amphiprion ocellaris). Mar. Freshw. Behav. Physiol. 50, 195–204.

Combalbert, S., Hernandez-Raquet, G., 2010. Occurrence, fate, and biodegradation of estrogens in sewage and manure. Appl. Microbiol. Biotechnol. 86, 1671–1692.

Silva, C.P., Otero, M., Esteves, V., 2012. Processes for the elimination of estrogenic steroid hormones from water: a review. Environ. Pollut. 165, 38–58.

Abdel-Fatah, M.A., 2018. Nanofiltration systems and applications in wastewater treatment. Ain Shams Eng. J. 9, 3077–3092.

Lipp, P., Sacher, F., Baldauf, G., 2010. Removal of organic micro-pollutants during drinking water treatment by nanofiltration and reverse osmosis. Desalin. Water Treat. 13, 226–237.

Visvanathan, C., Aim, R.B., Parameshwaran, K., 2000. Membrane separation bioreactors for wastewater treatment. Crit. Rev. Environ. Sci. Technol. 30, 1–48.

Bilal, M., Iqbal, H.M., 2019. Persistence and impact of steroidal estrogens on the environment and their laccase-assisted removal. Sci. Total Environ. 690, 447–459.

Akpotu, S.O., Lawal, I.A., Moodley, B., Ofomaja, A.E., 2020. Covalently linked graphene oxide/reduced graphene oxide-methoxylether polyethylene glycol functionalised silica for scavenging of estrogen: adsorption performance and mechanism. Chemosphere 246, 125729.

Larcher, S., Yargeau, V., 2013. The effect of ozone on the biodegradation of 17α-ethinylestradiol and sulfamethoxazole by mixed bacterial cultures. Appl. Microbiol. Biotechnol. 97, 2201–2210.

Puma, G.L., Puddu, V., Tsang, H.K., Gora, A., Toepfer, B., 2010. Photocatalytic oxidation of multicomponent mixtures of estrogens (estrone (E1), 17β-estradiol (E2), 17α-ethynylestradiol (EE2) and estriol (E3)) under UVA and UVC radiation: photon absorption, quantum yields and rate constants independent of photon absorption. Appl. Catal. B Environ. 99, 388–397.

Muruganathan, M., Yoshihara, S., Rakuma, T., Uehara, N., Shirakashi, T., 2007. Electrochemical degradation of 17β-estradiol (E2) at boron-doped diamond (Si/BDD) thin film electrode. Electrochim. Acta 52, 3242–3249.

Suri, R.P., Singh, T.S., Abburi, S., 2010. Influence of alkalinity and salinity on the sonochemical degradation of estrogen hormones in aqueous solution. Environ. Sci. Technol. 44, 1373–1379.

Schäfer, A., Nghiem, L., Waite, T., 2003. Removal of the natural hormone estrone from aqueous solutions using nanofiltration and reverse osmosis. Environ. Sci. Technol. 37, 182–188.

Jiang, L.-h., Liu, Y.-g., Zeng, G.-m., Xiao, F.-y., Hu, X.-j., Hu, X., Wang, H., Li, T.-t., Zhou, L., Tan, X.-f., 2016. Removal of 17β-estradiol by few-layered graphene oxide nanosheets from aqueous solutions: external influence and adsorption mechanism. Chem. Eng. J. 284, 93–102.

Ma, X., Zhang, C., Deng, J., Song, Y., Li, Q., Guo, Y., Li, C., 2015. Simultaneous degradation of estrone, 17β-estradiol and 17α-ethinyl estradiol in an aqueous UV/H2O2 system. Int. J. Environ. Res. Public Health 12, 12016–12029.

Yeh, T.F., Syu, J.M., Cheng, C., Chang, T.H., Teng, H., 2010. Graphite oxide as a photocatalyst for hydrogen production from water. Adv. Funct. Mater. 20, 2255–2262.

Talukdar, K., Jun, B.-M., Yoon, Y., Kim, Y., Fayyaz, A., Park, C.M., 2020. Novel Z-scheme Ag3PO4/Fe3O4-activated biochar photocatalyst with enhanced visible-light catalytic performance toward degradation of bisphenol A. J. Hazard. Mater. 123025.

Unuabonah, E.I., Agunbiade, F.O., Alfred, M.O., Adewumi, T.A., Okoli, C.P., Omorogie, M.O., Akanbi, M.O., Ofomaja, A.E., Taubert, A., 2017. Facile synthesis of new amino-functionalized agrogenic hybrid composite clay adsorbents for phosphate capture and recovery from water. J. Clean. Prod. 164, 652–663.

Cao, N., Zhang, Y., 2015. Study of reduced graphene oxide preparation by hummers' method and related characterization. J. Nanomater. 2015. doi:10.1155/2015/168125.

Azizi-Toupkanloo, H., Karimi-Nazarabad, M., Shakeri, M., Eftekhari, M., 2019. Photocatalytic mineralization of hard-degradable morphine by visible light-driven $Ag@gC_3N_4$ nanostructures. Environ. Sci. Pollut. Res. 1–13.

Karimi-Nazarabad, M., Goharshadi, E.K., 2017. Highly efficient photocatalytic and photoelectrocatalytic activity of solar light driven WO3/g-C3N4 nanocomposite. Sol. Energy Mater. Sol. Cells 160, 484–493.

Ugwuja, C.G., Adelowo, O.O., Ogunlaja, A., Omorogie, M.O., Olukanni, O.D., Ikhimiukor, O.O., Iermak, I., Kolawole, G.A., Guenter, C., Taubert, A., Bodede, O., Moodley, R., Inada, N.M., de Camargo, A.S.S., Unuabonah, E.I., 2019. Visible-light-Mediated photodynamic water disinfection@ bimetallic-doped hybrid clay nanocomposites. ACS Appl. Mater. Interfaces 11, 25483–25494.

Sharmila, T.B., Sasi, S., Suja, N., Beegum, P.S., Thachil, E.T., 2019. A comparative investigation of aminosilane/ethylene diamine–functionalized graphene epoxy nanocomposites with commercial and chemically reduced graphene: static and dynamic mechanical properties. Emerg. Mater. 1–16.

Bayode, A.A., Agunbiade, F.O., Omorogie, M.O., Moodley, R., Bodede, O., Unuabonah, E.I., 2020. Clean technology for synchronous sequestration of charged organic micro-pollutant onto microwave-assisted hybrid clay materials. Environ. Sci. Pollut. Res. 1–13.

Wang, F., Zhou, Y., Pan, X., Lu, B., Huang, J., Ye, Z., 2018. Enhanced photocatalytic properties of ZnO nanorods by electrostatic self-assembly with reduced graphene oxide. Phys. Chem. Chem. Phys. 20, 6959–6969.

de Campos Vidal, B., Mello, M.L.S., 2011. Collagen type I amide I band infrared spectroscopy. Micron 42, 283–289.

Sun, W., Shi, S., Yao, T., 2011. Graphene oxide–Ru complex for label-free assay of DNA sequence and potassium ions via fluorescence resonance energy transfer. Anal. Methods 3, 2472–2474.

Zhu, M., Lerum, M.Z., Chen, W., 2011. How to prepare reproducible, homogeneous, and hydrolytically stable aminosilane-derived layers on silica. Langmuir 28, 416–423.

Agawane, S.M., Nagarkar, J.M., 2012. Synthesis of 5-substituted 1 H-tetrazoles using a nano ZnO/Co 3 O 4 catalyst. Catal. Sci. Technol. 2, 1324–1327.

Fouad, D.E., Zhang, C., El-Didamony, H., Yingnan, L., Mekuria, T.D., Shah, A.H., 2019. Improved size, morphology and crystallinity of hematite (α-Fe2O3) nanoparticles synthesized via the precipitation route using ferric sulfate precursor. Results Phys. 12, 1253–1261.

Madejova, J., Komadel, P., 2001. Baseline studies of the clay minerals society source clays: infrared methods. Clays Clay Miner. 49, 410–432.

Jabbar, A., Yasin, G., Khan, W.Q., Anwar, M.Y., Korai, R.M., Nizam, M.N., Muhyodin, G., 2017. Electrochemical deposition of nickel graphene composite coatings: effect of deposition temperature on its surface morphology and corrosion resistance. RSC Adv. 7, 31100–31109.

Paz, S., Kahn, H., Angelica, R., 2018. A proposal for bauxite quality control using the combined Rietveld–le Bail–internal Standard PXRD Method–part 1: hkl model developed for kaolinite. Miner. Eng. 118, 52–61.

Berrier, E., Ovsitser, O., Kondratenko, E., Schwidder, M., Grünert, W., Brückner, A., 2007. Temperature-dependent N2O decomposition over Fe-ZSM-5: identification of sites with different activity. J. Catal. 249, 67–78.

Goldfarb, D., Bernardo, M., Strohmaier, K., Vaughan, D., Thomann, H., 1994. Characterization of iron in zeolites by X-band and Q-band ESR, pulsed ESR, and UV-visible spectroscopies. J. Am. Chem. Soc. 116, 6344–6353.

Guskos, N., Papadopoulos, G., Likodimos, V., Patapis, S., Yarmis, D., Przepiera, A., Przepiera, K., Majszczyk, J., Typek, J., Wabia, M., 2002. Photoacoustic, EPR and electrical conductivity investigations of three synthetic mineral pigments: hematite, goethite and magnetite. Mater. Res. Bull. 37, 1051–1061.

Mohanan, J.L., Arachchige, I.U., Brock, S.L., 2005. Porous semiconductor chalcogenide aerogels. Science 307, 397–400.

Fujimoto, A., Yamada, Y., Koinuma, M., Sato, S., 2016. Origins of sp3C peaks in C1s X-ray photoelectron spectra of carbon materials. Anal. Chem. 88, 6110–6114.

Zheng, Y., Qiao, L., Tang, J., Yang, Z., Yue, H., He, D., 2015. Electrochemically deposited interconnected porous Co 3 O 4 nanoflakes as anodes with excellent rate capability for lithium ion batteries. RSC Adv. 5, 36117–36121.

Karthik, R., Kumar, J.V., Chen, S.-M., Kumar, P.S., Selvam, V., Muthuraj, V., 2017. A selective electrochemical sensor for caffeic acid and photocatalyst for metronidazole drug pollutant-A dual role by rod-like SrV 2 O 6. Sci. Rep. 7, 1–12.

Yang, N., Zhai, J., Wang, D., Chen, Y., Jiang, L., 2010. Two-dimensional graphene bridges enhanced photoinduced charge transport in dye-sensitized solar cells. ACS Nano 4, 887–894.

Barroso-Bogeat, A., Alexandre-Franco, M., Fernandez-Gonzalez, C., Gomez-Serrano, V., 2019. Activated carbon surface chemistry: changes upon impregnation with Al (III), Fe (III) and Zn (II)-metal oxide catalyst precursors from NO3− aqueous solutions. Arab. J. Chem. 12, 3963–3976.

Lee, J., 2019. Metastable iron (iii) oxide polymorphs derived from Fe/Mn bimetallic coordination polymer particles in confined space: SiO 2 shell effect on crystal phase transition. CrystEngComm 21, 2849–2853.
Ching, J.Y., Huang, B.J., Hsu, Y.-T., Khung, Y.L., 2020. Anti-adhesion behavior from ring-strain amine cyclic monolayers grafted on silicon (111) surfaces. Sci. Rep. 10, 1–15.
Unuabonah, E.I., Gunter, C., Weber, J., Lubahn, S., Taubert, A., 2013. Hybrid clay: a new highly efficient adsorbent for water treatment. ACS Sustain. Chem. Eng. 1, 966–973.
Alshammari, A.S., Chi, L., Chen, X., Bagabas, A., Kramer, D., Alromaeh, A., Jiang, Z., 2015. Visible-light photocatalysis on C-doped ZnO derived from polymer-assisted pyrolysis. RSC Adv. 5, 27690–27698.
Meyers, K.S., Speyer, R.F., 2003. Thermal Analysis of Clays, Handbook of Thermal Analysis and Calorimetry. Elsevier, pp. 261–306.
Omorogie, M.O., Agunbiade, F.O., Alfred, M.O., Olaniyi, O.T., Adewumi, T.A., Bayode, A.A., Ofomaja, A.E., Naidoo, E.B., Okoli, C.P., Adebayo, T.A., Unuabonah, E.I., 2018. The sequestral capture of fluoride, nitrate and phosphate by metal-doped and surfactant-modified hybrid clay materials. Chem. Pap. 72, 409–417.
Melucci, M., Durso, M., Zambianchi, M., Treossi, E., Xia, Z.-Y., Manet, I., Giambastiani, G., Ortolani, L., Morandi, V., De Angelis, F., 2012. Graphene–organic hybrids as processable, tunable platforms for pH-dependent photoemission, obtained by a new modular approach. J. Mater. Chem. 22, 18237–18243.
Vallejo, W., Rueda, A., Díaz-Uribe, C., Grande, C., Quintana, P., 2019. Photocatalytic activity of graphene oxide–TiO_2 thin films sensitized by natural dyes extracted from *Bactris guineensis*. R. Soc. Open Sci. 6, 181824.
Chandraboss, V., Kamalakkannan, J., Prabha, S., Senthilvelan, S., 2015. An efficient removal of methyl violet from aqueous solution by an AC-Bi/ZnO nanocomposite material. RSC Adv. 5, 25857–25869.
Jiang, Z., Huang, B., Lou, Z., Wang, Z., Meng, X., Liu, Y., Qin, X., Zhang, X., Dai, Y., 2014. Immobilization of BiOX (X= Cl, Br) on activated carbon fibers as recycled photocatalysts. Dalton Trans. 43, 8170–8173.
ROSA, I.L.I., 2008. ABNT: Associação Brasileira de Normas Técnicas. Belo Horizonte: Faculdade Promove.
Coleman, H.M., Abdullah, M.I., Eggins, B.R., Palmer, F.L., 2005. Photocatalytic degradation of 17β-oestradiol, oestriol and 17α-ethynyloestradiol in water monitored using fluorescence spectroscopy. Appl. Catal. B Environ. 55, 23–30.
Kireesan, S., 2018. Photocatalytic Oxidation of Emerging Pollutants by Nano TiO_2.
Soltani, T., Entezari, M.H., 2013. Photolysis and photocatalysis of methylene blue by ferrite bismuth nanoparticles under sunlight irradiation. J. Mol. Catal. A Chem. 377, 197–203.
Zhang, J., Fu, D., Xu, Y., Liu, C., 2010. Optimization of parameters on photocatalytic degradation of chloramphenicol using TiO2 as photocatalyist by response surface methodology. J. Environ. Sci. 22, 1281–1289.
Kong, Y., Huang, Y., Meng, C., Zhang, Z., 2018. Sodium dodecylsulfate-layered double hydroxide and its use in the adsorption of 17β-estradiol in wastewater. RSC Adv. 8, 31440–31454.
Malygina, T., Preis, S., Kallas, J., 2005. The role of pH in aqueous photocatalytic oxidation of β-estradiol. Int. J. Photoenergy 7, 187–191.
Farner Budarz, J., Turolla, A., Piasecki, A.F., Bottero, J.-Y., Antonelli, M., Wiesner, M.R., 2017. Influence of aqueous inorganic anions on the reactivity of nanoparticles in TiO_2 photocatalysis. Langmuir 33, 2770–2779.
Tamirat, A.G., Rick, J., Dubale, A.A., Su, W.-N., Hwang, B.-J., 2016. Using hematite for photoelectrochemical water splitting: a review of current progress and challenges. Nanoscale Horiz. 1, 243–267.
Shown, I., Hsu, H.-C., Chang, Y.-C., Lin, C.-H., Roy, P.K., Ganguly, A., Wang, C.-H., Chang, J.-K., Wu, C.-I., Chen, L.-C., 2014. Highly efficient visible light photocatalytic reduction of CO2 to hydrocarbon fuels by Cu-nanoparticle decorated graphene oxide. Nano Lett. 14, 6097–6103.
Koe, W.S., Lee, J.W., Chong, W.C., Pang, Y.L., Sim, L.C., 2019. An overview of photocatalytic degradation: photocatalysts, mechanisms, and development of photocatalytic membrane. Environ. Sci. Pollut. Res. 1–44.
Simsek, E.B., Kilic, B., Asgin, M., Akan, A., 2018. Graphene oxide based heterojunction TiO2–ZnO catalysts with outstanding photocatalytic performance for bisphenol-A, ibuprofen and flurbiprofen. J. Ind. Eng. Chem. 59, 115–126.
Frontistis, Z., Drosou, C., Tyrovola, K., Mantzavinos, D., Fatta-Kassinos, D., Venieri, D., Xekoukoulotakis, N.P., 2012. Experimental and modeling studies of the degradation of estrogen hormones in aqueous TiO2 suspensions under simulated solar radiation. Ind. Eng. Chem. Res. 51, 16552–16563.
Jiang, J., Pang, S.-Y., Ma, J., Liu, H., 2012. Oxidation of phenolic endocrine disrupting chemicals by potassium permanganate in synthetic and real waters. Environ. Sci. Technol. 46, 1774–1781.
Deng, J., Tang, K., Zhu, S., Ma, X., Zhang, K., Song, Y., Li, X., Li, Q., Liu, Z., Zhou, K., 2015. Competitive degradation of steroid estrogens by potassium permanganate combined with ultrasound. Int. J. Environ. Res. Public Health 12, 15434–15448.